Synthesis and Crystal Structures of the Gold–Carbaborane Complexes [9-*exo*-{Au(PPh$_3$)}-9-(μ-H)-10-*endo*-{Au(PPh$_3$)}-7,8-Me$_2$-*nido*-7,8-C$_2$B$_9$H$_8$] and [10-*exo*-{Au$_2$(PPh$_3$)$_2$}-10-*endo*-{Au(PPh$_3$)}-7,8-Me$_2$-*nido*-7,8-C$_2$B$_9$H$_8$] *

John C. Jeffery,[a] Paul A. Jelliss[a,b] and F. Gordon A. Stone[b]
[a] *School of Chemistry, The University, Bristol BS8 1TS, UK*
[b] *Department of Chemistry, Baylor University, Waco, TX 76798-7348, USA*

Treatment of the salt [NEt$_4$][10-*endo*-{Au(PPh$_3$)}-7,8-Me$_2$-*nido*-7,8-C$_2$B$_9$H$_9$] with [AuCl(PPh$_3$)] in CH$_2$Cl$_2$ afforded the digold complex [9-*exo*-{Au(PPh$_3$)}-9-(μ-H)-10-*endo*-{Au(PPh$_3$)}-7,8-Me$_2$-*nido*-7,8-C$_2$B$_9$H$_8$]. Deprotonation of the latter with NaH in tetrahydrofuran followed by addition of [AuCl(PPh$_3$)] gave the trigold compound [10-*exo*-{Au$_2$(PPh$_3$)$_2$}-10-*endo*-{Au(PPh$_3$)}-7,8-Me$_2$-*nido*-7,8-C$_2$B$_9$H$_8$]. The crystal structures of the new compounds have been determined by X-ray diffraction. In the digold species one Au(PPh$_3$) group is *endo*-bound to the *nido*-C$_2$B$_9$ cage, primarily through a connectivity [Au–B 2.28(1) Å] with the boron atom which is in the β-site with respect to the two carbons in the open CCB*B*B face. There is a weaker attachment [Au–B 2.37(1) Å] to one of the α-boron atoms, while the other α-BH unit forms a three-centre two-electron B–H→Au bond with the second Au(PPh$_3$) group [Au–B 2.28(1), Au–μ-H 1.9(1) Å]. The latter gold fragment lies *exo* with respect to the open face of the carbaborane cage, with an Au–Au separation of 2.875(1) Å. The structure of the trigold complex is formally related to that of its digold precursor by replacement of the μ-H atom in the latter by an Au(PPh$_3$) moiety. This results in the molecule having an essentially isosceles triangle of gold atoms [Au–Au 2.691(1), 2.922(1), 3.010(1) Å], asymmetrically bridged by the β-boron [Au–B 2.192(9), 2.227(7), 2.307(8) Å] of the open CCB*B*B face of the C$_2$B$_9$ cage. The NMR data (^{1}H, ^{13}C-{^{1}H}, ^{31}P-{^{1}H} and ^{11}B-{^{1}H}) of the compounds are reported and discussed.

The anionic gold–carbaborane complexes [10-*endo*-{Au(PPh$_3$)}-7,8-R$_2$-*nido*-7,8-C$_2$B$_9$H$_9$]$^-$ (R = Me or H) are isolobal with the anions [10-*endo*-H-7,8-R$_2$-*nido*-7,8-C$_2$B$_9$H$_9$]$^-$ leading us to employ salts of the former species as reagents to prepare complexes in which gold is bonded to rhodium,[1a,b] iridium[1a,c] or platinum.[1d] During studies on the reaction between [NEt$_4$][10-*endo*-{Au(PPh$_3$)}-7,8-Me$_2$-*nido*-7,8-C$_2$B$_9$H$_9$] **1** and *trans*-[IrCl(CO)(PPh$_3$)$_2$], which gave as the major product (*ca.* 90% yield) the dimetal compound [1,2-Me$_2$-3-{Au(PPh$_3$)}-3-CO-3-(PPh$_3$)-*closo*-3,1,2-IrC$_2$B$_9$H$_9$], formation of a minor unidentified compound was observed.[1c] Further work established that this minor product was a trigold–carbaborane complex, and we describe herein its molecular structure and a rational synthesis from a digold precursor. The preparation and structure of the latter are also reported.

Results and Discussion

In CH$_2$Cl$_2$ the salt **1** and [AuCl(PPh$_3$)] react to give the digold complex [9-*exo*-{Au(PPh$_3$)}-9-(μ-H)-10-*endo*-{Au(PPh$_3$)}-7,8-Me$_2$-*nido*-7,8-C$_2$B$_9$H$_8$] **2**. Discussion of the NMR data for this product is deferred until the results of an X-ray diffraction study are described.

The molecule is shown in Fig. 1, and selected interatomic distances and angles are listed in Table 1. One Au(PPh$_3$) unit is *endo*-bonded to the open pentagonal face of the *nido*-C$_2$B$_9$ cage primarily through the connectivity between Au(1) and B(4) [2.28(1) Å] but with a somewhat weaker interaction with B(5) [2.37(1) Å]. The second Au(PPh$_3$) group has an *exo*-polyhedral relationship with the cage through the attachment to the B(3)H(3) vertex. The atom H(3) was directly located in Fourier difference syntheses, and its position refined, suggesting the existence of a three-centre two-electron B(3)–H(3)→Au(2) bond. Although, as discussed below, there was no NMR evidence for the μ-H(3) group, nevertheless, B–H→Au bonding is known in the complex [WRh$_2$Au$_2$(μ$_3$-CC$_6$H$_4$Me-4)(CO)$_6$(η-C$_5$H$_5$)(η^5-7,8-Me$_2$-7,8-C$_2$B$_9$H$_9$)$_2$] **3**.[2] In the latter species the two B–H→Au bonds have average Au–B separations of 2.37 Å, while the average Au–μ-H distance is 1.85 Å, based on their inclusion in calculated positions.[2] In compound **2** the Au(2)–μ-H(3) distance is 1.9(1) Å and the Au(2)–B(3) distance [2.28(1) Å] is shorter than the corresponding distances in **3**, implying a strong interaction between the gold atom and the BH group in the former species. In contrast, the complex [WRhAu(μ-CC$_6$H$_4$Me-4)(CO)$_3$(PPh$_3$)(η-C$_5$H$_5$)(η^5-7,8-C$_2$B$_9$H$_{11}$)] **4** has an Au[W(μ-CC$_6$H$_4$Me-4)(CO)$_2$(η-C$_5$H$_5$)] group which is bound to the rhodium atom of a *closo*-3,1,2-RhC$_2$B$_9$ cage. As expected, because there is no B–H→Au bonding in this complex, the separations of the gold atom from the boron atoms in the CCBBB pentagonal ring ligating the rhodium are appreciably greater (2.85–2.97 Å) than in **2**.

The Au(1)–Au(2) distance [2.875(1) Å] in compound **2** is very similar to that in elemental gold (2.884 Å) and within the range (2.60–3.10 Å) found in gold clusters of various types.[3] The metal–metal separation in **2** would be influenced by the steric and bonding requirements of the bridging carbaborane cage system. From a simple molecular orbital viewpoint, for a dimeric linear Au$_2$(PPh$_3$)$_2$ fragment, as discussed elsewhere,[4] the HOMO (highest occupied molecular orbital) is a σ$_g$ orbital, resulting from a combination of sp$_z$ orbitals on each gold, and leading to strong bonding between the metal atoms. The main bonding interaction between this digold unit and a 7,8-Me$_2$-

* *Supplementary data available:* see Instructions for Authors, *J. Chem. Soc., Dalton Trans.*, 1994, Issue 1, pp. xxiii–xxviii.

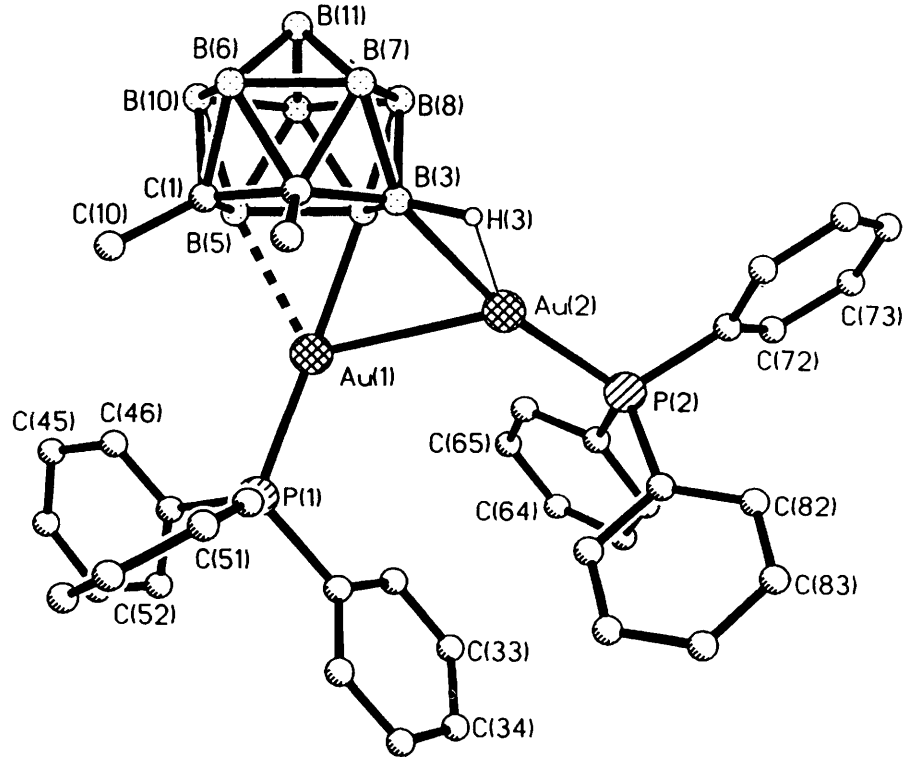

Fig. 1 The molecular structure of the complex [9-*exo*-{Au(PPh_3)}-9-(μ-H)-10-*endo*-{Au(PPh_3)}-7,8-Me_2-*nido*-7,8-$C_2B_9H_8$] **2** showing the crystallographic numbering scheme

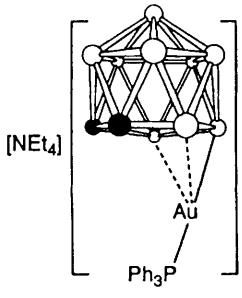

1 ○ BH ● CMe

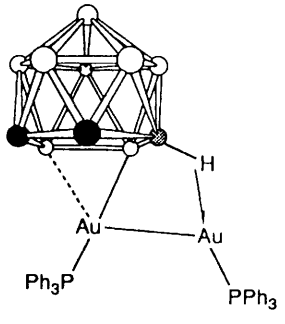

2 ○ BH ◍ B ● CMe

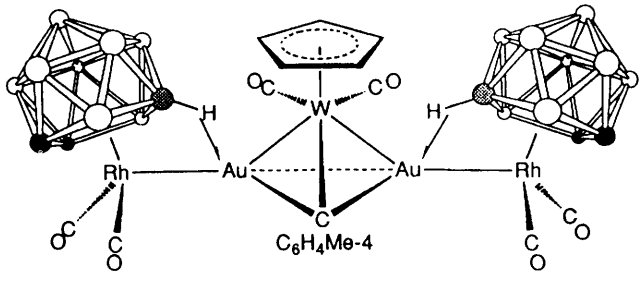

3 ○ BH ◍ B ● CMe

nido-7,8-$C_2B_9H_9$ cage in **2** might result from overlap of the filled σ_g orbital and a LUMO (lowest unoccupied molecular orbital) formed by a combination of orbitals on B(3), B(4) and B(5) in the face of the cage.[5] The $Au_2(PPh_3)_2$ unit is bent [P(1)–Au(1)–Au(2) 120.6(1), P(2)–Au(2)–Au(1) 123.0(1)°], which would weaken the Au–Au bond but enhance the bonding to the carbaborane group by increasing the overlap of the filled σ_g orbital of the digold moiety with the LUMO on the cage. Obviously, because of the observed unsymmetrical disposition of the Au(PPh_3) groups with respect to the cage in the solid state, the bonding is, in reality, more complicated. Furthermore, such a distortion of the $Au_2(PPh_3)_2$ group from linearity would

Table 1 Selected internuclear distances (Å) and angles (°) for the complex [9-*exo*-{Au(PPh$_3$)}-9-(μ-H)-10-*endo*-{Au(PPh$_3$)}-7,8-Me$_2$-*nido*-7,8-$C_2B_9H_8$] **2**

Au(1)–Au(2)	2.875(1)	Au(1)–P(1)	2.283(2)	Au(1)–B(4)	2.28(1)	Au(1)–B(5)	2.37(1)
Au(2)–P(2)	2.257(3)	Au(2)–B(3)	2.28(1)	Au(2)–H(3)	1.9(1)	C(1)–C(2)	1.57(1)
C(1)–B(5)	1.65(2)	C(1)–B(6)	1.74(2)	C(1)–B(10)	1.72(2)	C(1)–C(10)	1.52(2)
C(2)–B(3)	1.59(2)	C(2)–B(6)	1.71(2)	C(2)–B(7)	1.70(2)	C(2)–C(20)	1.52(2)
B(3)–B(4)	1.87(2)	B(3)–B(7)	1.78(2)	B(3)–B(8)	1.78(2)	B(3)–H(3)	1.20(9)
B(4)–B(5)	1.83(2)	B(4)–B(8)	1.82(2)	B(4)–B(9)	1.79(2)	B(4)–H(4)	1.1(1)
B(5)–B(9)	1.79(2)	B(5)–B(10)	1.79(2)	B(5)–H(5)	1.11(8)	B(6)–B(7)	1.73(2)
B(6)–B(10)	1.77(2)	B(6)–B(11)	1.78(2)	B(6)–H(6)	1.1(1)	B(7)–B(8)	1.77(2)
B(7)–B(11)	1.76(2)	B(7)–H(7)	1.21(9)	B(8)–B(9)	1.79(2)	B(8)–B(11)	1.79(2)
B(8)–H(8)	1.13(9)	B(9)–B(10)	1.73(2)	B(9)–B(11)	1.80(2)	B(9)–H(9)	1.0(1)
B(10)–B(11)	1.76(2)	B(10)–H(10)	1.0(1)	B(11)–H(11)	1.05(8)		

Au(2)–Au(1)–P(1)	120.6(1)	Au(2)–Au(1)–B(4)	61.8(3)	P(1)–Au(1)–B(4)	173.9(3)
Au(2)–Au(1)–B(5)	105.0(3)	P(1)–Au(1)–B(5)	133.2(3)	B(4)–Au(1)–B(5)	46.3(4)
Au(1)–Au(2)–P(2)	123.0(1)	Au(1)–Au(2)–B(3)	66.4(3)	P(2)–Au(2)–B(3)	169.3(3)
Au(1)–Au(2)–H(3)	94(3)	P(2)–Au(2)–H(3)	142(3)	B(3)–Au(2)–H(3)	32(3)
B(4)–Au(2)–H(3)	74(3)	Au(2)–B(3)–C(2)	139.9(7)	Au(2)–B(3)–B(4)	80.5(6)
Au(2)–B(3)–B(7)	154.8(8)	Au(2)–B(3)–B(8)	111.6(8)	Au(2)–B(3)–H(3)	57(5)
Au(1)–B(4)–B(3)	86.6(6)	Au(1)–B(4)–B(5)	69.6(5)	Au(1)–B(4)–B(8)	142.9(9)
Au(1)–B(4)–B(9)	128.7(8)	Au(1)–B(4)–H(4)	101(4)	Au(1)–B(5)–C(1)	93.4(6)
Au(1)–B(5)–B(4)	64.2(5)	C(1)–B(5)–B(4)	107.1(8)	Au(1)–B(5)–B(9)	123.4(8)
Au(1)–B(5)–B(10)	149.6(8)	Au(1)–B(5)–H(5)	97(5)	Au(2)–H(3)–B(3)	91(5)

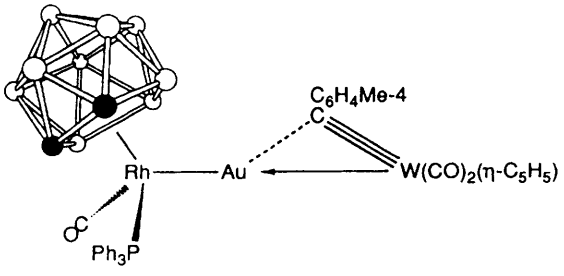

4 ○ BH ● CH

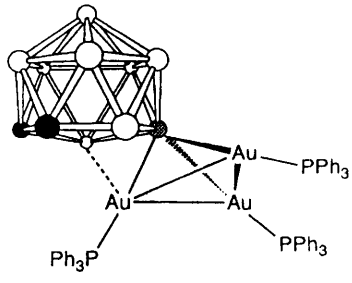

5 ○ BH ◍ B ● CMe

be sterically as well as electronically driven, in order to minimise the interaction between the carbaborane cage and the bulky PPh_3 ligands.

The NMR data (see Experimental section) for complex **2** reveal fluxional behaviour which persists at −80 °C. Even though the solid-state structure shows a lack of symmetry in the molecule, the ^{31}P-{^1H} NMR spectrum has only one broad resonance for the Au(PPh$_3$) groups, and the ^1H and ^{13}C-{^1H} NMR spectra indicate equivalence of the two cage CMe vertices. The unit cell in the crystal structure of **2** contains two enantiomers (Scheme 1, **I** and **II**), and in solution facile interconversion between the enantiomers could occur through the intermediacy of **III**, which has a plane of mirror symmetry. This low-energy process would average the NMR resonances for the Au(PPh$_3$) and CMe groups. Moreover, the fluxionality of the molecule might account for our inability to detect a resonance assignable to the B–H→Au group in either the ^1H or ^{11}B NMR spectra. In this context it may be noted that the ^1H NMR spectrum of the above-mentioned cluster compound **3** does not show resonances for B–H→Au groups though the presence of two such groups in this molecule was indicated in the X-ray diffraction study.[2]

It is interesting to compare the structure of compound **2** with the related dicopper complex [4,8-*exo*-{Cu(PPh$_3$)}-4,8-(μ-H)$_2$-3-(PPh$_3$)-*closo*-3,1,2-$CuC_2B_9H_9$].[6] In the latter molecule there is a Cu–Cu bond [2.576(1) Å], but one Cu(PPh$_3$) group functions as a vertex in a *closo*-3,1,2-CuC_2B_9 framework, while the other Cu(PPh$_3$) group forms two B–H→Cu bonds with two of the boron atoms of the open pentagonal CCBBB ring η^5-co-ordinated to the other copper atom. The preference shown by copper, compared with gold, to bond symmetrically (η^5 mode) has been demonstrated by Hamilton and Welch[5] and this preference is further indicated by the different structures of the digold and dicopper species compared here.

As mentioned in the Introduction, in the synthesis of [1,2-Me$_2$-3-{Au(PPh$_3$)}-3-CO-3-(PPh$_3$)-*closo*-3,1,2-$IrC_2B_9H_9$] a chromatographically inseparable minor side-product was observed. The nature of this species was resolved when the gold–iridium compound containing some of the minor product was treated with $PHPh_2$. Surprisingly, the major species isolated from this reaction was [1,2-Me$_2$-3-H-3-CO-3-(PPh$_3$)-*closo*-3,1,2-$IrC_2B_9H_9$], resulting from displacement of an Au(PPh$_3$) group from the iridium by $PHPh_2$. From the reaction mixture, however, crystals were grown of the minor compound initially present, and an X-ray diffraction study, described below, established this product as [10-*exo*-{Au$_2$(PPh$_3$)$_2$}-10-*endo*-{Au(PPh$_3$)}-7,8-Me$_2$-*nido*-7,8-$C_2B_9H_8$] **5**. It remained to devise a rational synthesis of the trigold complex **5**. This was accomplished by deprotonating thf (tetrahydrofuran) solutions of **2** with NaH to generate a carbaborane digold monoanion *in situ*, followed by treatment of the mixture with [AuCl(PPh$_3$)]. The structure of compound **5** is shown in Fig. 2, and selected structural parameters are listed in Table 2.

Three Au(PPh$_3$) groups in the molecule form an essentially isosceles triangle of gold atoms [Au(1)–Au(2) 2.691(1), Au(1)–Au(3) 3.010(1), Au(2)–Au(3) 2.922(1) Å]. This triangle is

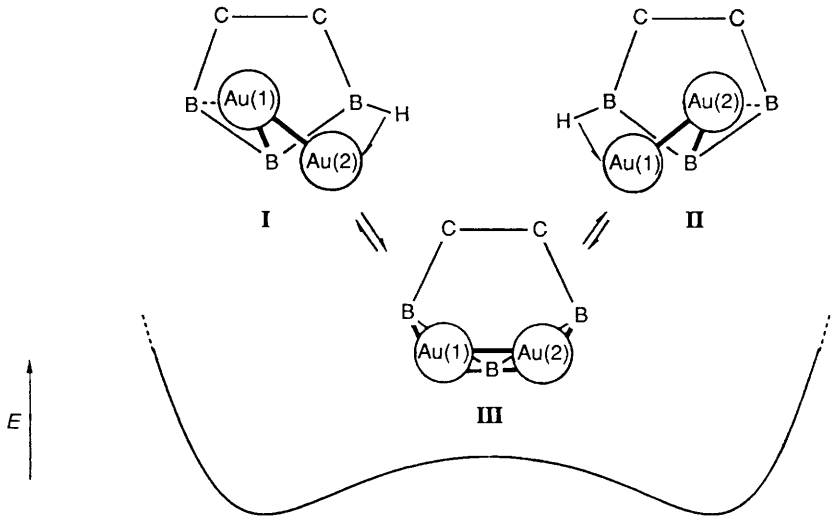

Scheme 1 Proposed pathway for the dynamic behaviour of compound **2** in solution

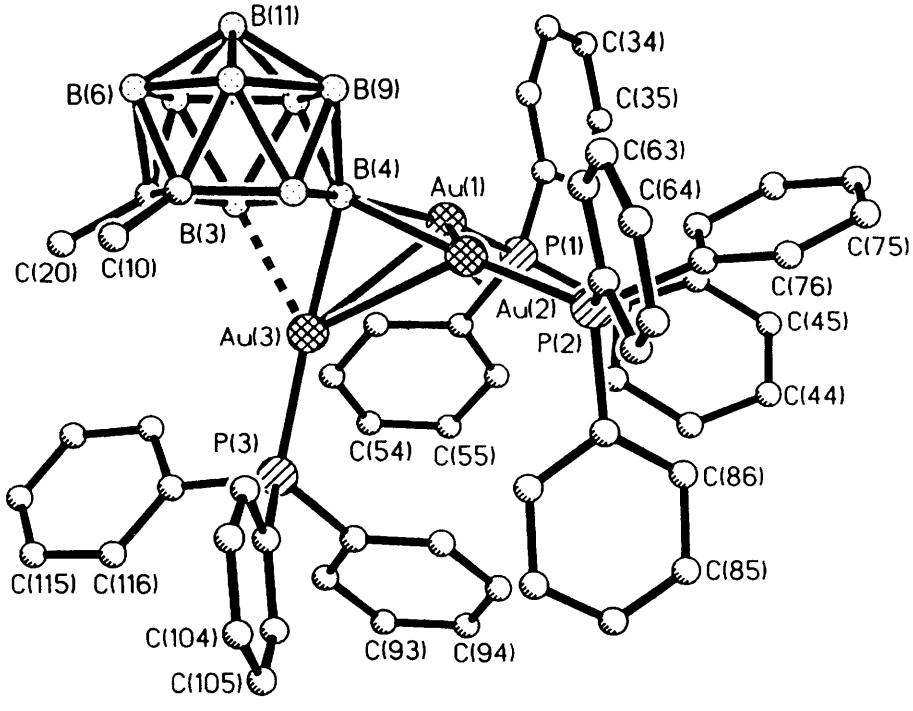

Fig. 2 The molecular structure of the complex [10-*exo*-{$Au_2(PPh_3)_2$}-10-*endo*-{$Au(PPh_3)$}-7,8-Me_2-*nido*-7,8-$C_2B_9H_8$] **5** showing the crystallographic numbering scheme

asymmetrically capped by B(4) [Au(1)–B(4) 2.227(7), Au(2)–B(4) 2.307(8), Au(3)–B(4) 2.192(9) Å], the boron atom in the β-site with respect to the two carbons in the open pentagonal CCB*B*B face of the *nido*-C_2B_9 cage. Interestingly the gold atom Au(3), *endo* to the face of the cage, and which forms the strongest connectivity with B(4), also has a weak attachment [2.403(9) Å] to B(3). This is reminiscent of atom Au(1) in the digold species **2** (Fig. 1), which is strongly linked with one boron atom in the face of the cage and more weakly attached to another. In complex **5**, in contrast with **2**, all the gold atoms share a common linkage with one boron atom [B(4)].

The separation [2.691(1) Å] between the gold atoms Au(1) and Au(2), which are *exo* to the face of the cage, is unusually short for a low-nuclearity gold cluster.[3] In the trigold complexes $[Au_3(\mu_3\text{-}O)(PPh_3)_3][BF_4]$[7] and $[Au_3(\mu_3\text{-}CPMe_3)(PPh_3)_3]$-Cl[8] the gold triangles are essentially symmetrically capped by the oxygen atom and the $CPMe_3$ groups, respectively, and the Au–Au separations are in the range 3.032–3.233 Å.

Compound **5** is not very soluble even in polar solvents like CH_2Cl_2. Nevertheless, it was possible to record NMR data from room temperature down to −70 °C. The measurements revealed that the molecule was highly fluxional. Thus the ^{31}P-{^1H} NMR spectrum displayed a single broad quartet at δ 39.3 [*J*(BP) 30 Hz] for the three $Au(PPh_3)$ groups throughout the temperature range, even though these groups are non-equivalent in the solid-state structure. Similarly, the ^1H and ^{13}C-{^1H} NMR spectra (see Experimental section) indicate that the cage CMe groups are equivalent even though from the X-ray diffraction study it is evident that they are not related by a molecular plane of symmetry. The fluxional behaviour of **5** can be accounted for by rotation of the C_2B_9 cage above the Au_3 triangle, as indicated in Scheme 2. This rotation would be accompanied by a breaking and reformation of the weak connectivity between a boron atom α to the two carbons and the *endo*-gold atom, as well as a concomitant contraction and expansion of the Au–Au bonds. Examination of the ^{11}B-{^1H} NMR spectrum of **5** revealed a doublet resonance corres-

Table 2 Selected internuclear distances (Å) and angles (°) for the complex [10-*exo*-{$Au_2(PPh_3)_2$}-10-*endo*-{$Au(PPh_3)$}-7,8-Me_2-*nido*-7,8-$C_2B_9H_8$] **5**

Au(1)–Au(2)	2.691(1)	Au(1)–Au(3)	3.010(1)	Au(1)–P(1)	2.289(2)	Au(1)–B(4)	2.227(7)
Au(2)–Au(3)	2.922(1)	Au(2)–P(2)	2.263(2)	Au(2)–B(4)	2.307(8)	Au(3)–P(3)	2.258(2)
Au(3)–B(3)	2.403(9)	Au(3)–B(4)	2.192(9)	B(3)–B(4)	1.85(1)	B(3)–B(7)	1.81(1)
B(3)–B(8)	1.81(1)	B(3)–H(3)	1.03(9)	B(3)–C(2)	1.64(1)	B(4)–B(5)	1.81(1)
B(4)–B(8)	1.78(1)	B(4)–B(9)	1.78(1)	B(5)–B(9)	1.79(1)	B(5)–B(10)	1.80(1)
B(5)–H(5)	0.99(9)	B(5)–C(1)	1.62(1)	B(6)–B(7)	1.75(1)	B(6)–B(10)	1.74(1)
B(6)–B(11)	1.74(1)	B(6)–H(6)	1.26(8)	B(6)–C(1)	1.75(1)	B(6)–C(2)	1.73(1)
B(7)–B(8)	1.80(1)	B(7)–B(11)	1.76(2)	B(7)–H(7)	1.11(9)	B(7)–C(2)	1.73(1)
B(8)–B(9)	1.80(1)	B(8)–B(11)	1.81(1)	B(8)–H(8)	1.18(8)	B(9)–B(10)	1.77(1)
B(9)–B(11)	1.80(1)	B(9)–H(9)	1.15(8)	B(10)–B(11)	1.76(2)	B(10)–H(10)	1.08(9)
B(10)–C(1)	1.76(2)	B(11)–H(11)	1.3(1)	C(1)–C(2)	1.55(1)	C(1)–C(10)	1.52(1)
C(2)–C(20)	1.53(1)						

Au(2)–Au(1)–Au(3)	61.4(1)	Au(2)–Au(1)–P(1)	135.1(1)	Au(3)–Au(1)–P(1)	125.6(1)
Au(2)–Au(1)–B(4)	55.0(2)	Au(3)–Au(1)–B(4)	46.6(2)	P(1)–Au(1)–B(4)	166.4(2)
Au(1)–Au(2)–Au(3)	64.7(1)	Au(1)–Au(2)–P(2)	132.4(1)	Au(3)–Au(2)–P(2)	135.8(1)
Au(1)–Au(2)–B(4)	52.2(2)	Au(3)–Au(2)–B(4)	47.8(2)	P(2)–Au(2)–B(4)	174.0(2)
Au(1)–Au(3)–Au(2)	53.9(1)	Au(1)–Au(3)–P(3)	133.4(1)	Au(2)–Au(3)–P(3)	126.2(1)
Au(1)–Au(3)–B(3)	72.4(2)	Au(2)–Au(3)–B(3)	98.3(2)	P(3)–Au(3)–B(3)	135.5(2)
Au(1)–Au(3)–B(4)	47.6(2)	Au(2)–Au(3)–B(4)	51.2(2)	P(3)–Au(3)–B(4)	176.8(2)
B(3)–Au(3)–B(4)	47.1(3)	Au(3)–B(3)–B(4)	60.4(4)	Au(3)–B(3)–B(7)	155.4(6)
Au(3)–B(3)–B(8)	117.7(5)	Au(3)–B(3)–C(2)	101.0(5)	Au(3)–B(3)–H(3)	90(5)
Au(1)–B(4)–Au(2)	72.8(2)	Au(1)–B(4)–Au(3)	85.9(3)	Au(2)–B(4)–Au(3)	81.0(3)
Au(1)–B(4)–B(3)	104.8(5)	Au(2)–B(4)–B(3)	153.5(6)	Au(3)–B(4)–B(3)	72.5(4)
Au(1)–B(4)–B(5)	152.9(5)	Au(2)–B(4)–B(5)	80.2(4)	Au(3)–B(4)–B(5)	91.8(5)
Au(1)–B(4)–B(8)	95.9(4)	Au(2)–B(4)–B(8)	145.9(5)	Au(3)–B(4)–B(8)	131.3(5)
Au(1)–B(4)–B(9)	121.6(4)	Au(2)–B(4)–B(9)	97.3(4)	Au(3)–B(4)–B(9)	151.0(5)

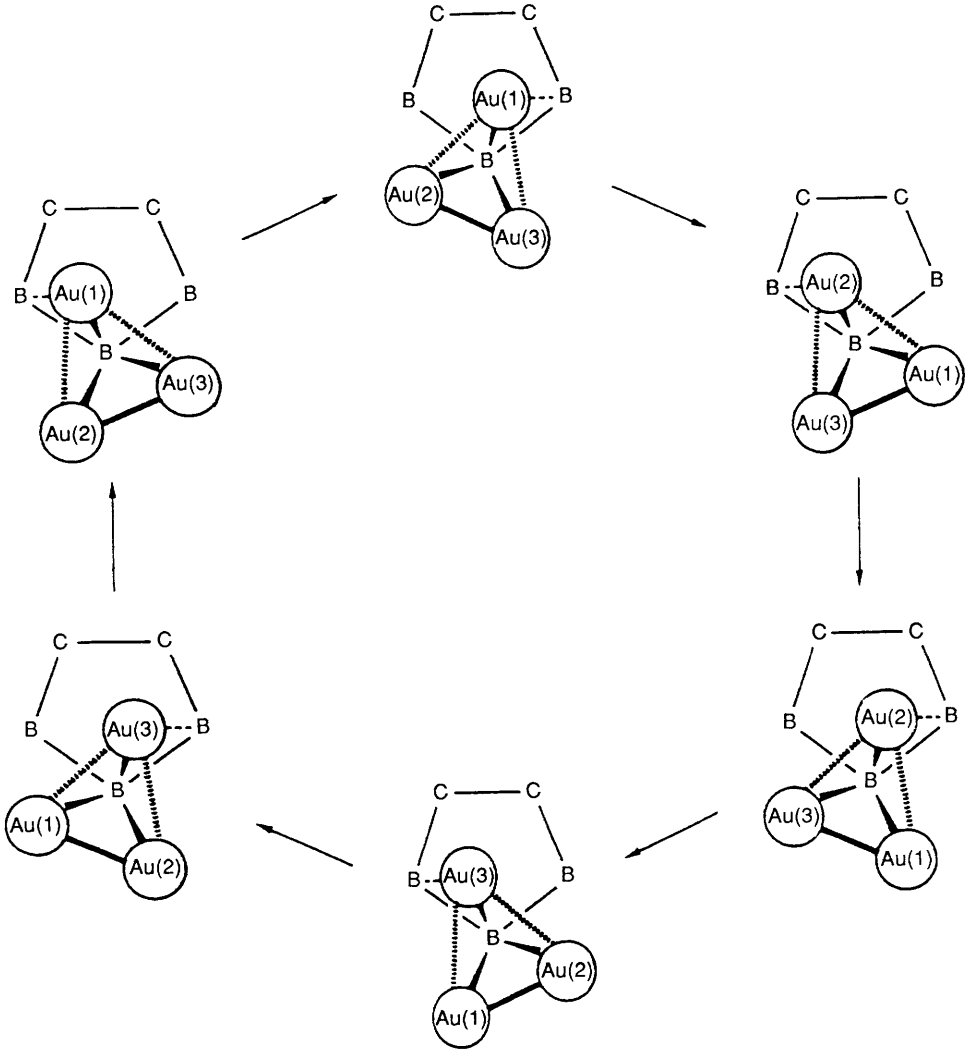

Scheme 2 Dynamic behaviour of complex **5** in solution. ——, Short Au–Au separation; ıılıı, longer Au–Au separation

ponding in intensity to one boron nucleus at δ −11.3 [J(PB) 30 Hz]. This signal must be assigned to the capping boron B(4) (Fig. 2).

The two compounds **2** and **5** have unprecedented structures in the rich field of metallacarbaborane complex chemistry. The unusual structures are undoubtedly influenced by the propensity of $Au(PPh_3)$ groups to form multicentre bonds.

Experimental

General experimental procedures and the instrumentation used have been described previously as has the preparation of the salt $[NEt_4][10\text{-}endo\text{-}\{Au(PPh_3)\}\text{-}7,8\text{-}Me_2\text{-}nido\text{-}7,8\text{-}C_2B_9H_9]$ **1**.[1b] The compound $[AuCl(PPh_3)]$ was obtained by the method reported elsewhere.[9] Light petroleum refers to that fraction of b.p. 40–60 °C. All NMR measurements (400 MHz for ^1H) were at ambient temperature in CD_2Cl_2, unless otherwise stated. Chemical shifts are in ppm, and coupling constants in Hz. The $^{31}P\text{-}\{^1H\}$ NMR (161.9 MHz) shifts are positive to high frequency of 85% H_3PO_4 (external), and the $^{11}B\text{-}\{^1H\}$ (128.3 MHz) shifts are positive to high frequency of $BF_3{\cdot}Et_2O$ (external).

Syntheses.—$[9\text{-}exo\text{-}\{Au(PPh_3)\}\text{-}9\text{-}(\mu\text{-}H)\text{-}10\text{-}endo\text{-}\{Au(PPh_3)\}\text{-}7,8\text{-}Me_2\text{-}nido\text{-}7,8\text{-}C_2B_9H_8]$. A mixture of the reagent **1** (0.16 g, 0.21 mmol) and $[AuCl(PPh_3)]$ (0.11 g, 0.21 mmol) was dissolved in CH_2Cl_2 (20 cm^3) and stirred at room temperature for *ca.* 12 h. Solvent was then reduced in volume *in vacuo* to *ca.* 3 cm^3, and the solution chromatographed on silica (2 × 15 cm column) at −40 °C. Elution with CH_2Cl_2–light petroleum, initially 2:3 and increasing gradually to neat CH_2Cl_2, removed a broad yellow band. Solvent was removed *in vacuo*, and the residue crystallised from CH_2Cl_2–light petroleum (1:4, 10 cm^3) to give yellow *microcrystals* of $[9\text{-}exo\text{-}\{Au(PPh_3)\}\text{-}9\text{-}(\mu\text{-}H)\text{-}10\text{-}endo\text{-}\{Au(PPh_3)\}\text{-}7,8\text{-}Me_2\text{-}nido\text{-}7,8\text{-}C_2B_9H_8]$ **2** (0.16 g, 74%) (Found: C, 44.9; H, 4.3. $C_{40}H_{45}Au_2B_9P_2$ requires C, 44.5; H, 4.2%). NMR: ^1H, δ 1.17 (s, 6 H, CMe) and 7.25–7.56 (m, 30 H, Ph); $^{13}C\text{-}\{^1H\}$ (in $CDCl_3$), δ 134.0 [d, C^2 of Ph, J(PC) 14], 131.3 (C^4 of Ph), 130.2 [d, C^1 of Ph, J(PC) 54], 129.0 [d, C^3 of Ph, J(PC) 12 Hz], 61.2 (br, *C*Me) and 22.8 (C*Me*); $^{31}P\text{-}\{^1H\}$, δ 38.1 (s, br, AuP); $^{11}B\text{-}\{^1H\}$ (all peaks broad), δ −9.1 (1 B), −12.5 (2 B), −15.3 (2 B), −16.4 (2 B), −27.0 (1 B) and −32.8 (1 B).

$[10\text{-}exo\text{-}\{Au_2(PPh_3)_2\}\text{-}10\text{-}endo\text{-}\{Au(PPh_3)\}\text{-}7,8\text{-}Me_2\text{-}nido\text{-}7,8\text{-}C_2B_9H_8]$. Compound **2** (0.20 g, 0.19 mmol) was dissolved in thf (15 cm^3) in a jacketed Schlenk tube, and cooled to −20 °C. A thf (5 cm^3) suspension of NaH (0.01 g, 0.25 mmol) was syringed into the reaction vessel, the contents of which were stirred vigorously. The mixture was then treated with $[AuCl(PPh_3)]$ (0.10 g, 0.20 mmol) in thf (10 cm^3) and the stirring continued for another 10 min. The reaction mixture was then slowly warmed to room temperature with stirring. Solvent was removed *in vacuo*, and the residue taken up in CH_2Cl_2 (30 cm^3) and filtered through a Celite pad (*ca.* 3 cm thick). The filtrate was reduced in volume *in vacuo* to *ca.* 4 cm^3 and chromatographed on silica at −40 °C. Elution with CH_2Cl_2–hexane, initially 1:1 and increasing to 9:1, removed a yellow fraction. Solvent was removed *in vacuo*, and the residue crystallised from CH_2Cl_2–hexane (1:3, 10 cm^3) to give yellow *microcrystals* of $[10\text{-}exo\text{-}\{Au_2(PPh_3)_2\}\text{-}10\text{-}endo\text{-}\{Au(PPh_3)\}\text{-}7,8\text{-}Me_2\text{-}nido\text{-}7,8\text{-}C_2B_9H_8]$ **5** (0.19 g, 65%) (Found: C, 46.1; H, 3.5. $C_{58}H_{59}Au_3B_9P_3$ requires C, 45.3; H, 3.9%). NMR: ^1H, δ 1.24 (s, 6 H, CMe) and 7.15–7.50 (m, 45 H, Ph); $^{13}C\text{-}\{^1H\}$, δ 134.7–129.1 (Ph), 58.0 (br, *C*Me) and 22.1 (C*Me*); $^{31}P\text{-}\{^1H\}$, δ 39.3 [q, br, AuP, J(BP) 30]; $^{11}B\text{-}\{^1H\}$ (all peaks broad), δ −5.3 (1 B), −11.3 [d, 1 B, BAu_3, J(PB) 30 Hz], −15.1 (2 B), −16.0 (2 B), −19.6 (2 B) and −36.3 (1 B).

Crystal Structure Determinations.—The crystal data and experimental parameters for compounds **2** and **5** are given in Table 3. Crystals of both **2** and **5** were grown by diffusion of hexane into CH_2Cl_2 solutions of the compounds. Compound **2** crystallises with one molecule of CH_2Cl_2 and half a molecule of hexane in the asymmetric unit, and rapid solvent loss occurs shortly after the crystals are removed from solution. The selected crystal was quickly mounted in a sealed glass capillary under nitrogen saturated with CH_2Cl_2–hexane (1:1). The selected crystal of compound **5** was also mounted in a sealed glass capillary under nitrogen. Both the crystals survived intact for the duration of the data collection with no significant loss of intensity recorded for the check reflections. All data were corrected for Lorentz, polarisation and X-ray absorption effects, the latter by an empirical method based upon azimuthal scan data.[10] The structures were solved by conventional heavy-atom methods and successive Fourier difference syntheses were used to locate all non-hydrogen atoms.

For compound **2** all non-hydrogen atoms were refined with anisotropic thermal parameters with the exception of the CH_2Cl_2–carbon atom, C(100), and the carbon atoms of the hexane, C(101)–C(105), which were refined with isotropic thermal parameters. Methyl and phenyl hydrogen atoms were included in calculated positions (C–H 0.96 Å) with fixed isotropic thermal parameters (U_{iso} = 0.08 $Å^2$). The cage BH hydrogen atoms, including the agostic B(3)–H(3)→Au(2) hydrogen, were all located in final electron-density difference maps and their positions refined with fixed isotropic thermal parameters (U_{iso} = 0.05 $Å^2$). As mentioned above, the asymmetric unit contains one molecule of CH_2Cl_2, the constituent chlorine and carbon atoms of which had respectively large anisotropic and isotropic thermal parameters. Also within the asymmetric unit is half a disordered hexane molecule. This molecule lies across a centre of inversion which is coincident

Table 3 Crystallographic data[a]

Compound	**2**	**5**
Crystal dimensions/mm	0.30 × 0.30 × 0.35	0.13 × 0.34 × 0.50
Molecular formula	$C_{40}H_{45}Au_2B_9P_2{\cdot}CH_2Cl_2{\cdot}0.5C_6H_{14}$[b]	$C_{58}H_{59}Au_3B_9P_3$
M	1207.0	1537.2
Crystal colour, shape	Yellow prism	Yellow rhomb
a/Å	9.289(3)	11.733(2)
b/Å	13.569(4)	13.120(3)
c/Å	20.248(6)	19.722(7)
α/°	78.65(2)	91.17(2)
β/°	84.70(2)	90.31(2)
γ/°	72.55(2)	109.07(2)
U/$Å^3$	2386(1)	2878(1)
D_c/ g cm^{-3}	1.68	1.77
μ(Mo-Kα)/cm^{-1}	63.5	77.5
F(000)	1170	1468
No. of reflections collected	11 987	14 444
No. of observed data used	6883	9312
Criterion for data (n) used $[F_o \geqslant n\sigma(F_o)]$	3	5
R (R')[c]	0.054 (0.045)	0.040 (0.041)
Final electron-density difference features (maximum, minimum)/ e $Å^{-3}$	1.20, −1.33	1.82, −1.86

[a] Data collected on a Siemens R3m/V four-circle diffractometer operating in the Wyckoff ω-scan mode; graphite-monochromated Mo-Kα X-radiation, $\bar{\lambda}$ = 0.710 73 Å. Refinement was by full-matrix least squares with a weighting scheme of the form $w^{-1} = [\sigma^2(F_o) + g|F_o|^2]$ with g = 0.0003 (**2**), 0.0007 (**5**); $\sigma^2(F_o)$ is the variance in F_o due to counting statistics; g was chosen so as to minimise variation in $\Sigma w(|F_o| - |F_c|)^2$ with $|F_o|$. Details in common: crystal system, triclinic; space group $P\bar{1}$; Z = 2; T = 293 K; data collection limits 2θ = 5–55°. [b] Asymmetric unit contains one molecule of CH_2Cl_2 and half a molecule of hexane, see text. [c] $R = \Sigma||F_o| - |F_c||/\Sigma|F_o|$, $R' = \Sigma w^{\frac{1}{2}}||F_o| - |F_c||/\Sigma w^{\frac{1}{2}}|F_o|$.

Table 4 Atomic positional parameters (fractional coordinates $\times 10^4$) for compound **2**, with estimated standard deviations (e.s.d.s) in parentheses

Atom	*x*	*y*	*z*	Atom	*x*	*y*	*z*
Au(1)	1763(1)	399(1)	1999(1)	C(53)	−3546(19)	1481(15)	556(8)
Au(2)	1684(1)	130(1)	3445(1)	C(54)	−4210(17)	988(13)	1094(10)
P(1)	111(3)	1802(2)	1379(1)	C(55)	−3573(17)	732(12)	1705(8)
P(2)	1557(3)	1443(2)	4001(1)	C(56)	−2281(15)	978(10)	1793(6)
C(1)	2027(12)	−1773(8)	1827(5)	C(61)	2437(12)	2413(7)	3544(5)
C(2)	1305(12)	−1868(8)	2561(5)	C(62)	2083(13)	3408(8)	3707(5)
B(3)	2053(13)	−1391(8)	3052(6)	C(63)	2767(15)	4156(9)	3345(7)
B(4)	3611(14)	−923(9)	2568(5)	C(64)	3741(13)	3903(9)	2838(7)
B(5)	3395(14)	−1206(10)	1741(6)	C(65)	4123(13)	2922(9)	2670(6)
B(6)	2393(15)	−3012(10)	2325(6)	C(66)	3478(12)	2175(8)	3008(5)
B(7)	2489(15)	−2775(10)	3127(7)	C(71)	2427(11)	981(8)	4812(5)
B(8)	3957(14)	−2188(9)	3129(6)	C(72)	3403(18)	1410(10)	5035(7)
B(9)	4797(15)	−2087(10)	2296(7)	C(73)	3956(20)	1051(12)	5674(7)
B(10)	3841(16)	−2599(11)	1819(7)	C(74)	3617(17)	248(12)	6085(6)
B(11)	4177(16)	−3216(10)	2664(7)	C(75)	2732(19)	−214(13)	5870(7)
C(10)	1028(15)	−1581(10)	1236(6)	C(76)	2097(17)	148(10)	5238(6)
C(20)	−377(13)	−1760(10)	2629(7)	C(81)	−384(11)	2180(8)	4162(4)
C(31)	−573(13)	3052(8)	1679(5)	C(82)	−1039(13)	2307(9)	4799(5)
C(32)	436(14)	3456(9)	1899(5)	C(83)	−2547(16)	2810(11)	4857(6)
C(33)	−23(19)	4416(11)	2111(7)	C(84)	−3416(17)	3240(13)	4309(7)
C(34)	−1489(20)	4981(10)	2105(6)	C(85)	−2798(14)	3148(12)	3674(7)
C(35)	−2551(16)	4594(9)	1882(6)	C(86)	−1304(13)	2622(10)	3600(5)
C(36)	−2092(13)	3627(9)	1668(5)	C(100)*	7560(25)	5778(19)	3988(10)
C(41)	940(12)	2141(8)	550(4)	Cl(1)*	6826(10)	5675(6)	4759(4)
C(42)	606(18)	3156(11)	201(7)	Cl(2)*	9146(9)	5970(7)	3878(6)
C(43)	1291(22)	3386(12)	−423(7)	C(101)*	4003(46)	3755(34)	773(20)
C(44)	2262(19)	2614(14)	−708(6)	C(102)*	3565(63)	4774(45)	897(23)
C(45)	2558(15)	1605(12)	−385(6)	C(103)*	2685(67)	5409(50)	773(29)
C(46)	1894(14)	1384(10)	245(5)	C(104)*	3935(119)	5329(79)	508(49)
C(51)	−1602(12)	1499(8)	1234(5)	C(105)*	4347(59)	4799(47)	262(28)
C(52)	−2264(16)	1733(12)	631(6)				

* Solvent molecule.

Table 5 Atomic positional parameters (fractional coordinates $\times 10^4$) for compound **5**, with e.s.d.s in parentheses

Atom	*x*	*y*	*z*	Atom	*x*	*y*	*z*
Au(1)	3254(1)	1384(1)	3099(1)	C(61)	3925(7)	2348(6)	110(4)
Au(2)	3009(1)	1432(1)	1744(1)	C(62)	4432(9)	1546(8)	−6(6)
Au(3)	764(1)	589(1)	2483(1)	C(63)	4677(11)	1297(10)	−665(7)
P(1)	3889(2)	2657(2)	3954(1)	C(64)	4386(10)	1778(9)	−1198(6)
P(2)	3762(2)	2748(2)	986(1)	C(65)	3850(9)	2547(10)	−1094(5)
P(3)	−781(2)	1251(2)	2471(1)	C(66)	3618(8)	2837(8)	−441(5)
B(3)	1140(7)	−925(7)	2985(5)	C(71)	5306(7)	3589(6)	1224(4)
B(4)	2281(6)	−30(6)	2435(4)	C(72)	5693(8)	3576(7)	1880(5)
B(5)	1779(8)	−680(7)	1616(5)	C(73)	6880(9)	4152(9)	2067(6)
B(6)	1019(9)	−2770(7)	2163(5)	C(74)	7651(8)	4739(8)	1585(7)
B(7)	1376(8)	−2222(8)	2983(5)	C(75)	7260(8)	4742(8)	929(6)
B(8)	2644(8)	−1004(7)	2926(5)	C(76)	6097(8)	4181(7)	758(6)
B(9)	3038(7)	−860(7)	2047(5)	C(81)	2875(7)	3651(6)	939(4)
B(10)	2027(9)	−1964(7)	1595(5)	C(82)	1662(8)	3210(8)	768(6)
B(11)	2524(9)	−2184(7)	2405(6)	C(83)	958(9)	3869(10)	732(7)
C(1)	649(7)	−1760(6)	1744(4)	C(84)	1447(11)	4942(10)	890(6)
C(2)	302(6)	−1918(6)	2501(4)	C(85)	2602(11)	5390(8)	1031(6)
C(10)	−353(9)	−2151(8)	1216(6)	C(86)	3343(9)	4746(7)	1068(5)
C(20)	−1019(8)	−2435(7)	2685(6)	C(91)	−545(7)	2576(7)	2858(5)
C(31)	5043(7)	2510(7)	4520(5)	C(92)	−1232(12)	2733(9)	3376(7)
C(32)	5525(9)	1724(9)	4390(6)	C(93)	−1033(15)	3779(10)	3660(8)
C(33)	6428(11)	1578(13)	4792(7)	C(94)	−129(13)	4621(10)	3432(9)
C(34)	6861(10)	2264(12)	5331(7)	C(95)	574(11)	4474(9)	2912(8)
C(35)	6392(10)	3048(11)	5485(6)	C(96)	360(9)	3442(7)	2634(6)
C(36)	5474(9)	3198(8)	5088(5)	C(101)	−1354(7)	1309(6)	1627(5)
C(41)	4487(8)	3998(7)	3615(5)	C(102)	−1119(8)	650(8)	1122(5)
C(42)	3734(11)	4341(9)	3198(7)	C(103)	−1581(10)	626(9)	477(6)
C(43)	4110(14)	5344(11)	2903(7)	C(104)	−2242(10)	1246(10)	315(6)
C(44)	5286(16)	6033(10)	3026(7)	C(105)	−2471(11)	1921(10)	799(7)
C(45)	6010(12)	5709(9)	3425(7)	C(106)	−2020(9)	1943(8)	1462(6)
C(46)	5648(9)	4705(8)	3722(6)	C(111)	−2048(6)	360(6)	2937(5)
C(51)	2609(7)	2701(8)	4467(5)	C(112)	−1801(9)	−142(9)	3495(7)
C(52)	1638(9)	1765(10)	4492(6)	C(113)	−2757(12)	−840(10)	3864(7)
C(53)	653(11)	1781(13)	4877(8)	C(114)	−3872(13)	−987(12)	3674(9)
C(54)	628(11)	2649(15)	5216(8)	C(115)	−4118(9)	−553(15)	3127(8)
C(55)	1545(13)	3585(14)	5167(8)	C(116)	−3216(7)	171(10)	2750(6)
C(56)	2582(10)	3616(11)	4792(7)				

with the centre of the middle C–C bond. The terminal ethyl fragment can apparently occupy one of two possible configurations within the asymmetric unit. This fragment was treated by assigning fixed site-occupancy factors of 0.5 to the methyl carbon atom positions of C(101) and C(103) and to the methylene carbon atom positions of C(102) and C(104). The remaining 'pivot' carbon atom, C(105), of this half of the molecule was refined with a fixed site-occupancy factor of 1.0. This solvent molecule is so severely disordered that the isotropic thermal parameters for the constituent carbon atoms are correspondingly large and subsequently no calculated hydrogen atoms were assigned to these carbon atoms.

For compound **5** all non-hydrogen atoms were refined with anisotropic thermal parameters. Methyl and phenyl hydrogen atoms were included in calculated positions (C–H 0.96 Å) with fixed isotropic thermal parameters (U_{iso} = 0.08 Å^2). The cage BH hydrogen atoms were located in final electron-density difference maps and their positions refined with fixed isotropic thermal parameters (U_{iso} = 0.05 Å^2). All computations were performed on a DEC μ-Vax II computer with the SHELXTL system of programs.[10] Scattering factors with corrections for anomalous dispersion were taken from ref. 11 and atomic coordinates are listed in Tables 4 and 5.

Additional material available from the Cambridge Crystallographic Data Centre comprises H-atom coordinates, thermal parameters, and remaining bond lengths and angles.

Acknowledgements

We thank the SERC for the award of a research studentship (to P. A. J.), and the Robert A. Welch Foundation for support (Grant AA-1201).

References

1 (*a*) J. A. K. Howard, J. C. Jeffery, P. A. Jelliss, T. Sommerfeld and F. G. A. Stone, *J. Chem. Soc., Chem. Commun.*, 1991, 1664; (*b*) J. C. Jeffery, P. A. Jelliss and F. G. A. Stone, *J. Chem. Soc., Dalton Trans.*, 1993, 1073; (*c*) J. C. Jeffery, P. A. Jelliss and F. G. A. Stone, *J. Chem. Soc., Dalton Trans.*, 1993, 1083; (*d*) J. C. Jeffery, P. A. Jelliss and F. G. A. Stone, *Inorg. Chem.*, 1993, **32**, 3943.
2 N. Carr, M. C. Gimeno, J. E. Goldberg, M. U. Pilotti, F. G. A. Stone and I. Topaloğlu, *J. Chem. Soc., Dalton Trans.*, 1990, 2253.
3 K. P. Hall and D. M. P. Mingos, *Prog. Inorg. Chem.*, 1984, **32**, 237.
4 D. I. Gilmour and D. M. P. Mingos, *J. Organomet. Chem.*, 1986, **302**, 127.
5 E. J. M. Hamilton and A. J. Welch, *Polyhedron*, 1990, **9**, 2407.
6 H. C. Kang, Y. Do, C. B. Knobler and M. F. Hawthorne, *Inorg. Chem.*, 1988, **27**, 1716.
7 A. N. Nesmeyanov, E. G. Perevalova, Yu. T. Struchkov, M. Yu. Antipin, K. I. Grandberg and V. P. Dyadchenko, *J. Organomet. Chem.*, 1980, **201**, 343.
8 H. Schmidbaur, F. Scherbaum, B. Huber and G. Müller, *Angew. Chem., Int. Ed. Engl.*, 1988, **27**, 419.
9 R. Usón and A. Laguna, *Organomet. Synth.*, 1986, **3**, 325.
10 G. M. Sheldrick, SHELXTL programs for use with a Siemens X-ray system, University of Cambridge, 1976, updated University of Göttingen, 1981.
11 *International Tables for X-Ray Crystallography*, Kynoch Press, Birmingham, 1974, vol. 4.

Received 24*th May* 1993; *Paper* 3/02943C